IMPROVING THE CALCULATION OF THE POTENTIAL BETWEEN SPHERICAL AND DEFORMED NUCLEI

M. Ismail and Kh.A. Ramadan

Physics Department, Faculty of Science, Cairo University
Giza, Egypt

(Received March 3, 1999; revised version received November 17, 1999)

The Heavy Ion (HI) interaction potential between spherical and deformed nuclei is improved by calculating its exchange part using finite range nucleon–nucleon (NN) force. We considered U^{238} as a target nucleus and seven projectile nuclei to show the dependence of the HI potential on both the energy and orientation of the deformed target nucleus. The effect of finite range NN force has been found to produce significant changes in the HI potential. The variation of the barrier height V_B, its thickness and its position R_B due to the use of finite range NN force are significant. Such variation enhance the fusion cross-section at energy values just below the Coulomb barrier by a factor increasing with the mass number of projectile nucleus.

PACS numbers: 21.30.Fe

1. Introduction

The static and dynamic deformations give rise to significant changes in the Coulomb and nuclear energies. The nuclear structure aspects of inelastic scattering are contained in the so-called form factors of the transition potentials coupling various nuclear levels. The form factor depends sensitively on the static and dynamic deformation [1]. Moreover, the deformation of the target and projectile affects both fusion reaction [2] and deep inelastic scattering [3]. The sub barrier fusion enhancement observed in heavy ion reactions is explained by allowing the relative motion degree of freedom to couple with internal degrees of freedom, as static deformation [4]. Since the main part in calculating the cross-section for heavy ion reaction is the nucleus–nucleus interaction potential (U), many authors have studied and derived the orientation and deformation dependence of the potential between deformed–deformed [5,6] and deformed spherical nuclei [7]. Some of these studies have been made in the framework of the energy density formalism [6] and others within the well known double folding model [5,8]. In the double folding model, the real optical potential is the sum of direct and exchange parts. In the simplest version of this model, the exchange part is calculated approximately by assuming zero-range nucleon–nucleon (NN) force [8]. The exchange part of the real HI interaction potential is obtained by applying the Pauli principle on the interacting nucleons. Improvement of the calculation of this part is made by considering finite range NN force instead of the zero-range pseudo-potential. In this case the problem of calculating the real optical potential becomes self-consistent problem and the HI potential becomes energy dependent [9]. More than ten years ago [10], the exchange HI interaction potential for spherical nuclei has been calculated using finite range NN force. It was found that the more accurate treatment of the exchange part affects both the internal and surface regions of the HI interaction potential, and moreover it produces energy dependence.

In the present work we aim to improve HI interaction potential for spherical-deformed nuclear pair by calculating its exchange part using finite range NN force. We shall consider the U^{238} nucleus as a target and the seven nuclei C^{12}, O^{16}, Ar^{40}, Ca^{40}, Ni^{64}, Zr^{90} and Pb^{208} as projectiles. We study both the energy and orientation dependence to the HI potential for the above mentioned pairs.

In Section 2 we describe the method used to calculate the real potential for deformed-spherical nuclear pair. Section 3 is left for presenting and discussing the obtained results. We give a summary in Section 4.

2. The interaction potential between deformed and spherical nuclei

In the double folding model, the interaction potential between a deformed target nucleus and a spherical projectile with separation distance R between their centers is given by

$$U(R,\,\beta) = U_D(R,\,\beta) + U_{\rm ex}(R,\,\beta)\,, \tag{1}$$

where β is the orientation angle of the deformed nucleus with respect to R. U_D and $U_{\rm ex}$ are the direct and exchange parts of the real potential, respectively. They are given by [9, 10]

$$U_D(R,\,\beta) = \int d\boldsymbol{r}_1 d\boldsymbol{r}_2 \rho_1(\boldsymbol{r}_1)\rho_2(\boldsymbol{r}_2)V_D(\boldsymbol{s})\,, \tag{2}$$

$$U_{\rm ex}(R,\,\beta) = \int d\boldsymbol{r}_1 d\boldsymbol{r}_2 \rho_1(\boldsymbol{r}_1,\boldsymbol{r}_1+\boldsymbol{s})\rho_2(\boldsymbol{r}_2,\boldsymbol{r}_2-\boldsymbol{s})V_{\rm ex}(\boldsymbol{s})\exp\frac{i\boldsymbol{k}\cdot\boldsymbol{s}}{M} \tag{3}$$

with $\boldsymbol{s} = \boldsymbol{R} + \boldsymbol{r}_2 - \boldsymbol{r}_1$ and $V_D(\boldsymbol{s})$ and $V_{\rm ex}(\boldsymbol{s})$ are the direct and exchange parts of the nucleon–nucleon force, respectively, ρ_1 and ρ_2 denote the mass distribution in the target and projectile nuclei. The non-diagonal density $\rho_j(\boldsymbol{r}, \boldsymbol{r}')$ is given in terms of the single particle wave functions ϕ_i as:

$$\rho_j(\boldsymbol{r}, \boldsymbol{r}') = \sum_i \phi_i^*(\boldsymbol{r}) \phi_i(\boldsymbol{r}') \,. \tag{4}$$

The local wave number $|\boldsymbol{k}|$ is given by:

$$|\boldsymbol{k}|^2 = \left(\frac{2\mu}{\hbar^2}\right) \Big(E_{\rm C.M.} - U(\boldsymbol{R}, \beta) - U_c(\boldsymbol{R}, \beta)\Big) \tag{5}$$

with $\mu = M_1 M_2/(M_1 + M_2)$, U_c is the Coulomb potential for the two interacting ions and $E_{\rm C.M.}$ the energy in the center of mass system. The energy in laboratory system $E_{\rm L}$ is given by $E_{\rm L} = ((M_1 + M_2)/M_2) E_{\rm C.M.}$, M_1 and M_2 denote the masses of the projectile and target, respectively.

The method of calculating U_D and U_c is outlined in Ref. [5]. In the simple version of the double folding model, the exchange part is usually simplified by expressing $V_{\rm ex}(\boldsymbol{s})$ in terms of δ-function. For M3Y-Reid version of the NN force, $V_{\rm ex}(\boldsymbol{s})$ is approximated by [8]:

$$V_{\rm ex}(\boldsymbol{s}) = -276 \left(1 - 0.005 \frac{E_{\rm L}}{A_1}\right) \delta(\boldsymbol{s}) \,, \tag{6}$$

where $(E_{\rm L}/A_1)$ is the incident energy in laboratory system per projectile nucleon. A_1 is the mass number of the projectile.

Recently [9–11], many authors calculated the exchange part of the HI potential for spherical nuclei using finite range NN exchange force. In this approach the non-diagonal matrices are approximated by the density matrix expansion (DME) method [12] as:

$$\rho_j(\boldsymbol{r}, \boldsymbol{r} + \boldsymbol{s}) = \rho_j\left(\boldsymbol{r} + \tfrac{1}{2}\boldsymbol{s}\right) \hat{j}_1(k_{{\rm eff}(j)}(\boldsymbol{r} + \tfrac{1}{2}\boldsymbol{s}) s) \tag{7}$$

with

$$\hat{j}_1(x) = 3 \frac{\sin x - x \cos x}{x^3}$$

and

$$k^2_{{\rm eff}(j)}(r) = \left(\frac{5/3}{\rho_j(\boldsymbol{r})}\right) \left[\tau_j(\boldsymbol{r}) - \left(\frac{1}{4}\right) \nabla^2 \rho_j(\boldsymbol{r})\right] , \ (j = 1, 2) \,. \tag{7a}$$

The best approximation for τ_j is the extended Thomas–Fermi approximation given by

$$\tau(\boldsymbol{r}) = \frac{3}{5} k_f^2 \rho(\boldsymbol{r}) + \frac{1}{3} \nabla^2 \rho(\boldsymbol{r}) + \frac{1}{36} \frac{|\bar{\nabla} \rho(\boldsymbol{r})|^2}{\rho(\boldsymbol{r})} \,. \tag{7b}$$

The DME method is a good approximation for heavy nuclei and for M3Y nucleon–nucleon force [13].

For spherical nuclei the density distribution is assumed to be

$$\rho(\boldsymbol{r}) = \frac{\rho_0}{1 + \exp\frac{r - r_0}{a}}\,. \tag{8}$$

The density distribution of the deformed nucleus is usually taken as

$$\rho(r,\theta) = \frac{\rho_0}{1 + \exp\frac{r - R(\theta)}{a}}\,. \tag{9}$$

The half density radius of this Fermi distribution is given by

$$R(\theta) = R_0[1 + \delta_2 Y_{20}(\theta,0) + \delta_4 Y_{40}(\theta,0]\,, \tag{10}$$

where δ_2 and δ_4 are the quadrupole and hexadecapole deformation parameters, respectively, and the angle θ is measured from the symmetry axis of the deformed nucleus. The values of the parameters r_0 and a for spherical nucleus is taken from Ref. [8]. The values of the parameters R_0, a, δ_2 and δ_4 for the deformed nucleus are taken from Ref. [14], ρ_0 is determined from the relation

$$\int \rho(\boldsymbol{r}) d\boldsymbol{r} = \text{mass number of the nucleus}\,.$$

Referring to Fig. 1 $U_{\text{ex}}(R,\beta)$ is given by

$$\begin{aligned} U_{\text{ex}}(R,\beta) &= \int d\boldsymbol{s} \exp\frac{i\boldsymbol{k}\boldsymbol{s}}{M} V_{\text{ex}}(s) \int d\boldsymbol{y} \rho_1(\boldsymbol{y}) \\ &\quad \times \hat{j}_1(k_{\text{eff}(1)}(\boldsymbol{y})s))\rho_2(|\boldsymbol{y} - \boldsymbol{R}|)\hat{j}_1(k_{\text{eff}(2)}(|\boldsymbol{y} - \boldsymbol{R}|)s))\,. \end{aligned} \tag{11}$$

Defining

$$\begin{aligned} G(R,\beta,s) &= \int \rho_1(y,\cos(\theta))\hat{j}_1(k_{\text{eff}(1)}(y,\cos\theta)s) \\ &\quad \times \rho_2(x)\hat{j}_1(k_{\text{eff}(2)}(x)s) y^2 \sin\theta d\theta d\phi dy\,, \end{aligned} \tag{12}$$

where $x = |\boldsymbol{y} - \boldsymbol{R}|$. In terms of $G(R,\beta,s)$ equation (11) becomes

$$U_{\text{ex}}(R,\beta) = \int d\boldsymbol{s} \exp\frac{i\boldsymbol{k}\boldsymbol{s}}{M} V_{\text{ex}}(s) G(R,\beta,s)\,. \tag{13}$$

For the interaction between two spherical nuclei, the quantity $G(R,\beta,s)$ is replaced by

$$G(R,s) = 2\pi \int \rho_1(y) j_1(k_{\text{eff}(1)}(y)s)\rho_2(x) j_1(k_{\text{eff}(2)}(x)s) y^2 dy \sin\theta d\theta\,, \tag{14}$$

and $U_{\rm ex}(R)$ becomes

$$U_{\rm ex}(R) = \int d\boldsymbol{s} \exp \frac{i\boldsymbol{ks}}{M} V_{\rm ex}(s) G(R,s)\,. \tag{15}$$

The value of $G(R,s)$ in equation (14) is obtained at each value of s and R by calculating two-dimensional integral. For the interaction between deformed-spherical pair $G(R,\beta,s)$ depends on the orientation angle β of the deformed nucleus. It can be calculated by performing the three-dimensional integral of equation (12) at each value of s and R. In the two types of interacting nuclei, G is independent on both the energy and the total potential $U(R,\beta)$. Performing the angular integration of s in equation (13), one gets,

$$U_{\rm ex}(R,\beta) = 4\pi \int ds s^2 j_0\left(\frac{ks}{M}\right) V_{\rm ex}(s) G(R,\beta,s)\,. \tag{16}$$

The nucleon–nucleon potential used in the present calculations is the well known M3Y–Reid NN force [15], whose direct and exchange parts are

$$V_D(s) = 7999\frac{\exp(4s)}{-4s} - 2134\frac{\exp(-2.5s)}{2.5s}\,, \tag{17a}$$

$$V_{\rm ex}(s) = 4631.4\frac{\exp(-4s)}{4s} - 1787.1\frac{\exp(-2.5s)}{2.5s} - 7.847\frac{\exp(-0.7072s)}{0.7072s}\,. \tag{17b}$$

It should be noted that the calculation of $U(R,\beta)$ using finite range exchange NN force is a self consistent problem due to the appearance of $U(R,\beta)$ in equation (5). This problem is solved by iteration method [16].

3. Numerical results and discussion

In the present work we considered the deformed nucleus U^{238} as a target and C^{12}, O^{16}, Ar^{40}, Ca^{40}, Ni^{64}, Zr^{90} and Pb^{208} as projectiles. We calculated the real part of the interaction potential for the first four nuclear pairs at three values of laboratory energy per projectile nucleon $E_L/A_1 = 5.2,\ 11.6$ and 20.7 MeV. In terms of the relative momentum per projectile nucleon, $k_r = \sqrt{2mE_L/\hbar^2 A_1}$, these energies correspond to the values $k_r = 0.5,\ 0.75$ and 1.00 fm^{-1}, respectively. For each nuclear pair considered in the present work we calculated the two quantities $U^{\delta}_{\rm ex}(R,\beta)$ and $U^{F}_{\rm ex}(R,\beta)$ using the zero-range NN force (Eq. (6)) and the finite-range force (Eq. (17b)), respectively. In the present work we have calculated both the direct part $U_{\rm D}$ and the Coulomb potential $U_{\rm C}$ using the procedure of Ref. [5]. The results are shown on figures 1–7 and Tables I–V.

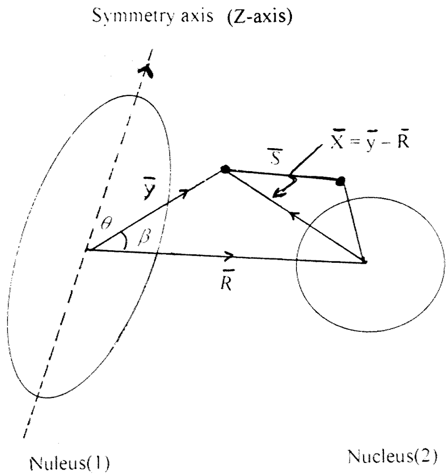

Fig. 1. Systematic representation of the two interacting deformed spherical nuclei. The x-axis is in the R–Z plane.

TABLE I

U^{238}–C^{12}

The height of the barrier $V_{\rm B}$ and its position $R_{\rm B}$ for U^{238}–C^{12} potential calculated at $k_r = 0.5,\ 0.75$ and 1 fm^{-1} using zero-range and finite-range exchange NN force. Three different relative orientations β =0°, 45°, 90° are considered. The table shows also the increase percentage of the diffusion cross-section σ_F calculated at four values of $E_{\rm C.M.}$ above the Coulomb barrier. The center of mass energies within k_r range (0.56–0.67 fm^{-1}).

k_r	β	Finite-range (Exact)		Zero-range App.)		Increase in σ_F %			
						$E_{\rm C.M.}$ (MeV)			
		$R_{\rm B}$	$V_{\rm B}$	$R_{\rm B}$	$V_{\rm B}$	75	85	95	105
0.5	0°	13.36	58.38	13.07	59.49	11.96	9.03	7.75	7.10
	45°	11.81	62.91	11.65	63.93	12.14	7.74	6.14	5.32
	90°	11.42	64.22	11.32	64.57	5.19	3.52	2.95	2.67
0.75	0°	13.34	58.52	13.07	59.52				
	45°	11.79	63.09	11.64	63.98				
	90°	11.39	64.36	11.31	64.62				
1	0°	13.29	58.71	13.05	59.58				
	45°	11.75	63.33	11.63	64.05				
	90°	11.36	64.55	11.30	64.69				

Tables I–IV show the Coulomb barrier parameters $R_{\rm B}$ and $V_{\rm B}$ for U^{238}–C^{12}, U^{238}–O^{16}, U^{238}–Ar^{40} and U^{238}–Ca^{40}, respectively at the three values of $E_L/A_1 = 5.2,\ 11.6$ and 20.7 MeV. Each table shows the values of

TABLE II

$U^{238}-O^{16}$

The same as Table I but for U^{238}–O^{16} pair. The center of mass energies within k_r range (0.55–0.63 fm^{-1}).

k_r	β	Finite-range (Exact)		Zero-range App.)		Increase in σ_F %			
						$E_{\mathrm{C.M.}}$ (MeV)			
		R_{B}	V_{B}	R_{B}	V_{B}	95	105	115	125
0.5	0°	13.60	76.41	13.26	77.96	14.76	11.22	9.60	8.66
	45°	12.25	82.19	12.03	83.40	14.51	9.50	7.68	6.71
	90°	11.71	83.51	11.52	84.26	10.54	7.06	5.85	5.23
0.75	0°	13.51	76.87	13.23	78.10				
	45°	12.16	82.66	11.99	83.54				
	90°	11.61	84.02	11.47	84.46				
1	0°	13.44	77.19	13.21	78.21				
	45°	12.10	82.99	11.98	83.65				
	90°	11.53	84.37	11.44	84.61				

TABLE III

$U^{238}-Ar^{40}$

The same as Table I but for U^{238}–Ar^{40} pair. The center of mass energies within k_r range (0.52–0.56 fm^{-1}).

k_r	β	Finite-range (Exact)		Zero-range App.)		Increase in σ_F %			
						$E_{\mathrm{C.M.}}$ (MeV)			
		R_{B}	V_{B}	R_{B}	V_{B}	190	200	210	220
0.5	0°	14.42	161.00	14.03	164.49	20.09	16.02	13.74	12.28
	45°	13.10	172.36	12.85	175.08	22.88	15.27	12.02	10.07
	90°	12.51	175.68	12.21	177.95	24.75	15.78	12.41	10.64
0.75	0°	14.38	161.45	14.02	164.62				
	45°	13.06	172.82	12.85	175.21				
	90°	12.45	176.19	12.19	178.14				
1	0°	14.31	162.06	14.00	164.81				
	45°	13.01	173.43	12.81	175.41				
	90°	12.38	176.83	12.16	178.41				

barrier parameters calculated, by using both finite range and zero range NN force. Table V presents the same quantities calculated at only one value of E_L/A_1 for the three pairs $U^{238}-Ni^{64}$, $U^{238}-Zr^{90}$ and $U^{238}-Pb^{208}$. Tables I–IV show a weak energy dependence of both R_{B} and V_{B} in the considered energy range. The effect of increasing E_L/A_1 is the slight decrease of R_{B} and increase of V_{B} by very small amount. These results agree with the energy dependence of the folding model for the interaction potential between spherical nuclei. This model produces weak energy dependence that makes the nuclear potential more repulsive as the projectile energy is increased.

TABLE IV

$U^{238}-Ca^{40}$

The same as Table I but for U^{238}–Ca^{40} pair. The center of mass energies within k_r range (0.54–0.58 fm^{-1}).

k_r	β	Finite-range (Exact)		Zero-range App.)		Increase in σ_F %			
						$E_{\text{C.M.}}$ (MeV)			
		R_{B}	V_{B}	R_{B}	V_{B}	210	220	230	240
0.5	0°	14.36	179.10	13.95	183.29	22.59	18.06	15.47	8.16
	45°	13.02	191.71	12.72	195.20	29.28	19.52	15.28	12.93
	90°	12.43	195.83	12.16	198.67	30.68	18.40	13.96	11.67
0.75	0°	14.24	180.36	13.91	183.68				
	45°	12.90	193.05	12.68	195.62				
	90°	12.31	197.24	12.11	199.16				
1	0°	14.16	181.24	13.88	183.98				
	45°	12.82	193.97	12.65	195.95				
	90°	12.23	198.21	12.08	199.56				

TABLE V

The same as Table I but for the three heavy projectile pairs $U^{238}-Ni^{64}$, $U^{238}-Zr^{90}$ and $U^{238}-Pb^{208}$. Only one value of $k_r (k_r = 0.5$ fm$^{-1})$ is considered. The center of mass energies withink_r range (0.52–0.56 fm^{-1}).

Pair	β	Finite-range (Exact)		Zero-range App.)		Increase in σ_F %			
						$E_{\text{C.M.}}$ (MeV)			
		R_{B}	V_{B}	R_{B}	V_{B}	285	295	305	315
U^{238}-Ni^{64}	0°	14.67	246.11	14.30	251.36	21.67	17.90	15.54	13.92
	45°	13.36	263.14	13.08	267.29	28.77	19.95	15.81	13.40
	90°	12.73	268.87	12.49	272.32	32.14	19.68	14.85	12.28
						380	390	400	410
U^{238}-Zr^{90}	0°	15.27	337.06	14.86	344.53	27.84	22.95	19.82	17.65
	45°	13.97	359.22	13.65	365.42	49.26	31.15	23.52	19.31
	90°	13.35	367.48	13.05	372.99	86.98	38.58	26.02	20.25
						690	700	710	720
U^{238}-Pb^{208}	0°	16.86	622.98	16.40	637.20	34.15	29.62	26.33	23.84
	45°	15.63	659.16	15.26	671.45	74.41	50.07	38.35	31.46
	90°	14.97	674.97	14.59	687.35	497.10	108.31	62.82	45.20

As an example to show the effect of the finite range NN force on the nuclear interaction potential for spherical-deformed nuclear pair, we considered the interacting pair U^{238}–Ca^{40}. Figure 2 shows our calculations for the total nuclear potential $U^{\delta} = U_D + U_{\text{ex}}^{(\delta)}$ and $U^F = U_D + U_{\text{ex}}^{(F)}$ for orientation angles $\beta = 0°$ and 90°. Fig. 2 indicates that the use of finite-range NN force reduces the attraction of U^{238}–Ca^{40} potential by about 17.5% at

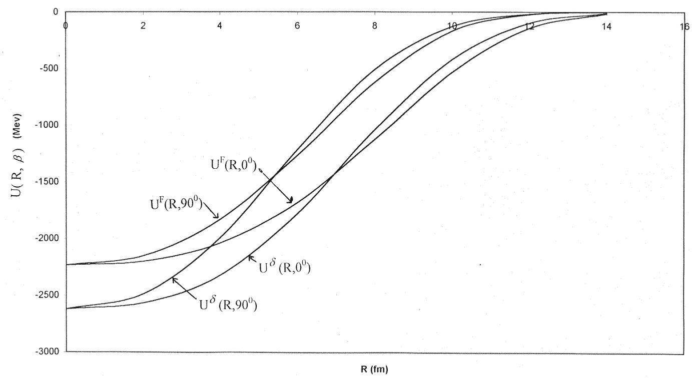

Fig. 2. The real part of the U^{238}–Ca^{40} nuclear potential for the two different relative orientations $\beta = 0°$ and 90° using finite-range NN interaction (U^F) and zero-range NN interaction (U^δ) against the separation distance R (fm) between the centers of the two interacting nuclei. Calculations have been done at incident energy in laboratory system per projectile nucleon $E_L/A_1 = 5.2$ MeV ($k_r = 0.5\ \mathrm{fm}^{-1}$)

.

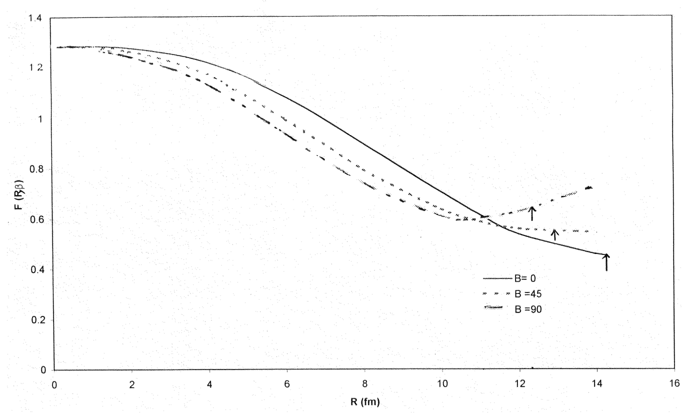

Fig.3a. The factor $F(R, \beta)$ for relative orientation $\beta = 0°$, 45° and 90°, against R (fm) at $k_r = 0.5\ \mathrm{fm}^{-1}$ for U^{238}–Ca^{40}. The arrows refer to the position of the barriers.

separation ion distance $R = 0$ fm and makes the potential deeper in a region before the surface region. This is clear in Fig. 3a which compares the factor $F(R, \beta) = U^\delta_{\mathrm{ex}}(R, \beta)/U^F_{\mathrm{ex}}(R, \beta)$ for U^{238}–Ca^{40} at the three values of orientation angle $\beta = 0°$, 45° and 90°. This figure shows that $|U^\delta_{\mathrm{ex}}|$ is greater than $|U^F_{\mathrm{ex}}|$ by about 30% at separation distance $R = 0 (F(0, \beta) = 1.3)$. As the value of R increases the factor $F(R, \beta)$ decreases for the two relative orientations $\beta = 0°$ and $\beta = 45°$. For $\beta = 90°$ the value of F decreases

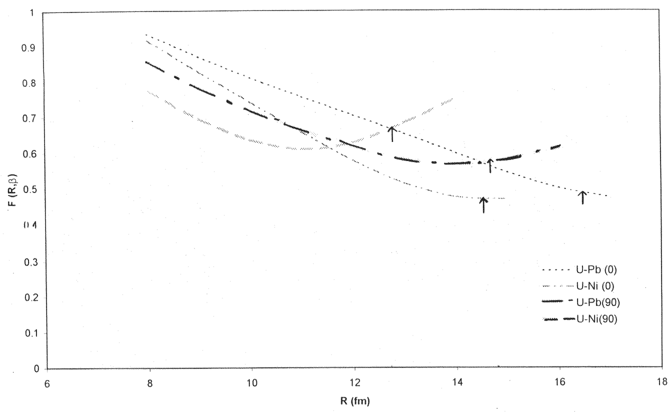

Fig.3b. The factor $F(R,\beta)$ for relative orientation $\beta = 0°$, $90°$, against R (fm) at $k_r = 0.5$ fm^{-1} for U^{238}–Pb^{208} and U^{238}–Ni^{64}. The arrows refer to the position of the barriers.

for $R < 10$ fm than it increases slowly. For fixed R value, the difference in shapes between the factor F is due to the difference in volume of the overlap region between the two nuclear densities when the orientation angle is varied. This is because $U_{\rm ex}^{\delta}$ is proportional to the volume of the overlap region of the two nuclear density distributions. Figure 3b shows the variation of the factors $F(R, 0)$ and $F(R, 90°)$ with the separation distance R for the heavier pairs U^{238}–Ni^{64} and U^{238}–Pb^{208}. The general behaviour of the factor F for these two pairs is the same as that for U^{238}–Ca^{40} pair.

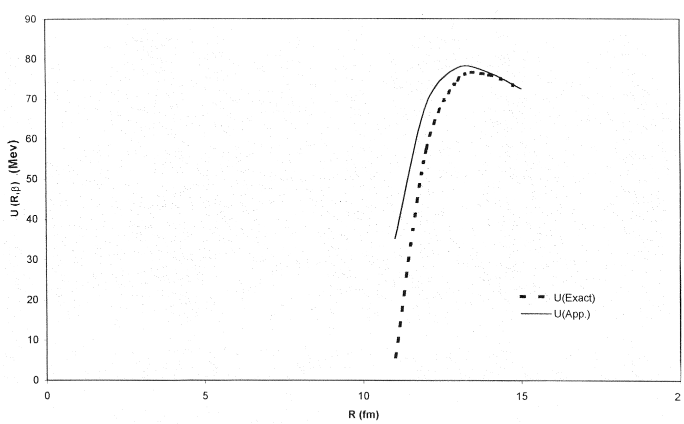

Fig.4a. The total U^{238}–O^{16} potential (both exact and approximate) against R (fm) at $k_r = 0.5$ fm^{-1} and for orientation angle $\beta = 0°$.

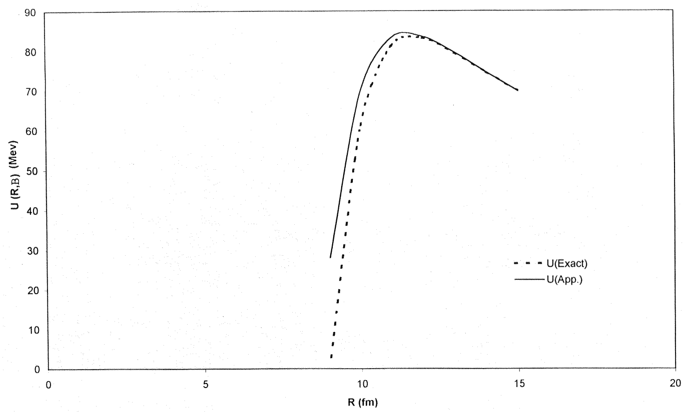

Fig.4b. The same as Fig. 4a but for $\beta = 90°$

Figures 4 and 5 show the total real potential, U_T (nuclear + Coulomb) for the two pairs U^{238}–O^{16} and U^{238}–Zr^{90}, respectively at $E_L/A_1 = 5.2$ MeV. Figure 4a shows U_T calculated using zero range and finite range NN forces at orientation angle $\beta = 0°$ for the nuclear pair U^{238}–O^{16}. Figure 4b is the same as figure 4a but for $\beta = 90°$. Figure 5 contains the same calculations for the pair U^{238}–Zr^{90}. These figures show that the finite range NN force affects the fusion barrier height ($V_{\rm B}$), its thickness and its position ($R_{\rm B}$). The effect is to increase the value of $R_{\rm B}$ and reduces the height of the barrier $V_{\rm B}$. This is shown in Tables I–V for three orientation angles $\beta = 0°$, $45°$ and $90°$, where the values of $R_{\rm B}$ and $V_{\rm B}$ calculated using both U^{δ} and U^{F} are presented for seven interacting pairs. For U^{238}–Ca^{40} pair and at $E_L/A_1 \cong 5.2$ MeV the increase in the value of $R_{\rm B}$ resulting from using finite range NN force in calculating the exchange part is 2.94%, 2.36% and 2.22% for $\beta = 0°$, $45°$ and $90°$, respectively. The corresponding decrease in $V_{\rm B}$ is 2.29%, 1.8% and 1.43% for the same values of β. For the other interacting nuclear pairs the percentage variation in $R_{\rm B}$ or $V_{\rm B}$ due to finite range NN force differs from that corresponding to Ca^{40}–Ca^{40} pair. In all cases it does not exceed 3%. For the HI potential between two deformed U^{238} nuclei it was found that [17] the correct treatment of $U_{\rm ex}$ reduces $V_{\rm B}$ by about 2.8% and shifts $R_{\rm B}$ outwards by a maximum value of 3.5%. The maximum shift in $R_{\rm B}$ for deformed–deformed nuclear pair increases by 12% comparing to the same quantity in the present work.

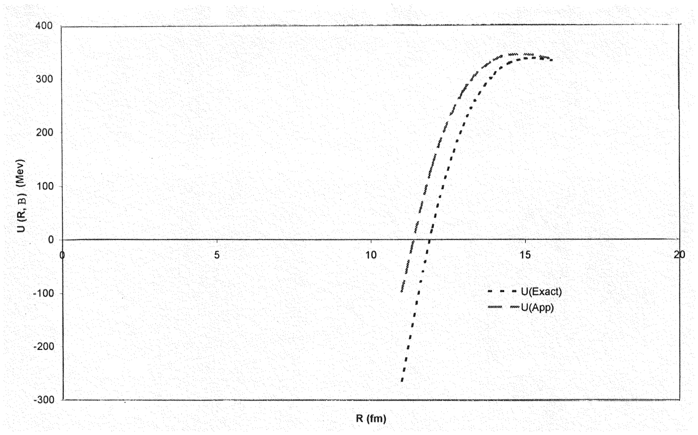

Fig.5a. The same as Fig. 4a but for the pair U^{238}–Zr^{90}

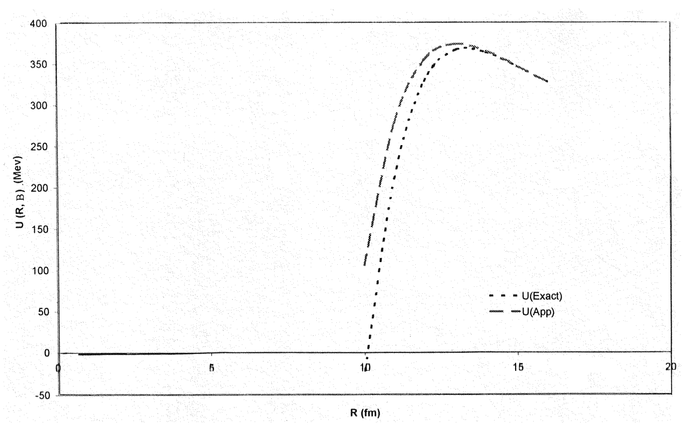

Fig.5b. The same as Fig. 4b but for the pair U^{238}–Zr^{90}

Although the changes in $R_{\rm B}$ and $V_{\rm B}$ resulting from using finite range NN force are small, they produce significant changes in the fusion cross section for energy values just below and above the Coulomb barrier. For this energy range the fusion cross-section can be calculated from the formula [18].

$$\sigma_F = \frac{R_{\rm B}^2 \hbar\omega}{2E_{\rm C.M.}} \ln\left[1 + \exp\left(\frac{2\pi(E_{\rm C.M.} - E_{\rm B})}{\hbar\omega}\right)\right] , \tag{18}$$

where

$$\hbar\omega = \hbar\left\{\left(\frac{d^2U_T}{dr^2}\right)_{R_{\rm B}} \frac{1}{\mu}\right\}^{1/2} .$$

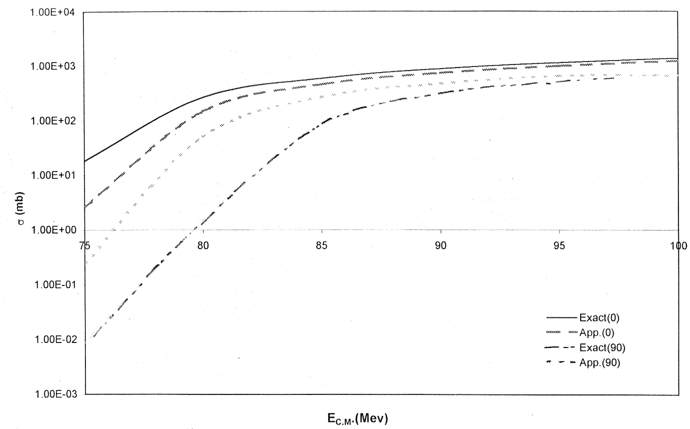

Fig.6. Variation of fusion cross-section σ_F for U^{238}–O^{16} reaction with $E_{\rm C.M.}$ for orientations $\beta = 0°$ and $90°$. σ_F has been calculated using finite range (exact) and zero range (approx.) NN force.

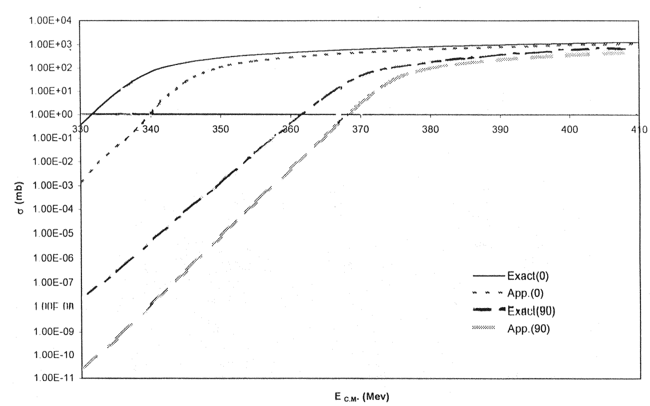

Fig.7. The same as Fig. 6 but for the pair U^{238}–Zr^{90}

This formula had been derived by approximating the Coulomb barrier by parabolic shape. It is valid if the difference between $E_{\rm C.M.}$ and the barrier top is relatively small. For heavy projectile (like Zr^{90}) the Coulomb barrier is about 350 MeV and it is expected that equation (18) can be used at energies less by 30–40 MeV than $V_{\rm B}$.

The effect of finite range NN force on the fusion cross-section is shown in the last column of Tables I–V and in Figs 6, 7. Each table contains the percentage increase of the fusion cross-section σ_F resulting from using finite range NN force instead of zero range force. Variation in σ_F was calculated at four values of $E_{\rm C.M.} > V_{\rm B}$. The tables show that the percentage increase in the calculated values of σ_F is significant for center of mass energy above the Coulomb barrier. As the projectile nucleus gets lighter the enhancement of σ_F is reduced. For example at energy $E_{\rm C.M.} \cong V_{\rm B} + 20$ MeV, where $V_{\rm B}$ calculated with zero range force and for $\beta = 0°$, the percentage increase in σ_F is about 14%, 28%, 33% and 46% for the projectiles O^{16}, Ca^{40}, Ni^{64} and Zr^{90}, respectively. This enhancement of σ_F resulting from the finite range of the exchange NN force is mainly due to the direct dependence of σ_F on $R_{\rm B}^2$ whose value increases with the projectile mass number.

To show the effect of using finite range force σ_F for energies just below and above the Coulomb barrier [19] we considered the interacting pairs U^{238}–O^{16} and U^{238}–Zr^{90} as examples. Figures 6 and 7 show the variation of σ_F with $E_{\rm C.M.}$ for the projectiles O^{16} and Zr^{90}, respectively. In each figure we considered the two U^{238} orientations angles $\beta = 0°$ and $90°$. The figures show that the finite range of the exchange NN force enhances σ_F, at energies just below the Coulomb barrier by a factor depends on the projectile mass number. Moreover, at a certain value of $E_{\rm C.M.}$ the finite range of the force has large effect on σ_F for $\beta = 90°$ compared to its effect on $\beta = 0°$.

4. Summary

We generalized the calculation of the real interaction potential using finite range NN exchange force to include deformation of the target nucleus. The effect of finite range of the force on the calculations of the interaction potential for deformed–spherical nuclear pair has been studied. We considered the U^{238} nucleus with both quadrupole and hexadecapole parameters and seven projectiles with mass numbers $12 \leq A_1 \leq 208$. It was found that the finite range NN force produces more repulsive HI potential at small separation distances and makes the potential more attractive in surface and tail regions. The fusion barrier parameters are affected by the finite range force. The barrier height is lowered and its position is shifted outwards compared with the same quantities calculated by zero range force. The energy dependence of the barrier parameters was found to be too small in the range of energy considered in the present work. We found that the fusion cross-section at energies just below and above the Coulomb barrier is enhanced by a factor increasing with the projectile mass number. Moreover this factor is strongly dependent on the orientation of U^{238} nucleus.

The effect found in the present paper is a result of the orientation dependence of the factor $F(R,\beta)$. The later depend on the overlap region between the density distributions of the two interacting nuclei which changes by the orientation of the target nucleus.

We wish to thank Dr A.Y. Ellithi for his help during the preparation of the manuscript.

REFERENCES

[1] V.E. Oberacker, M.J. Rhoades-Brown, G.R. Satchler, *Phys. Rev.* **C26**, 129 (1982).

[2] J.X. Wei *et al.*, *Phys. Rev. Lett.* **67**, 3368 (1991); J.D. Bierman *et al.*, *Phys. Rev.* **C54**, 3068 (1996).

[3] M. Munchow, W. Scheid, *Nucl. Phys.* **A286**, 59 (1978).

[4] R.G. Stokstad, Y. Eisen, S. Kaplains, D. Pelte, U. Smilansky, I. Tserruya, *Phys. Rev.* **C21**, 2427 (1980).

[5] M.J. Rhoadas-Brown, V.E. Oberacker, M. Seiwert, W. Griener, *Z. Phys.* **A310**, 287 (1983).

[6] M. Ismail, M. Rashdan, A. Faessler, M. Trefz, H.M. Mansour, *Z. Phys.* **A323**, 399 (1986).

[7] M. Rashdan, *J. Phys. G* **22**, 139 (1996).

[8] G.R. Satchler, W.G. Love, *Phys. Rep.* **55**, 183 (1979).

[9] D.T. Khoa *et al.*, *Phys. Rev. Lett.* **74**, 34 (1995); D.T. Khoa, W.V. Oertzen, *Phys. Lett.* **B342**, 6 (1995); D.T. Khoa, W.V. Oertzen, H.G. Bohlen, *Phys. Rev.* **C49**, 1652 (1994).

[10] A.K. Chaudhuri, B. Sinha, *Nucl. Phys.* **A455**, 169 (1986).

[11] D.T. Khoa, G.R. Satchler, W.V. Oertzen, *Phys. Rev.* **C56**, 954 (1997).

[12] X. Campi, A. Bouyssy, *Phys. Lett.* **B73**, 263 (1978).

[13] . Ismail, M. Osman, F. Salah, *Phys. Lett.* **B378**, 40 (1996).

[14] T. Cooper etal, *Phys. Rev.* **C13**, 1083 (1976).

[15] G. Bertsch, J. Borysowicz, H. Mc Manus, W.G. Love, *Nucl. Phys.* **A284**, 399 (1977).

[16] M. Ismail, *J. Phys.* (Paris) **32**, 729 (1971).

[17] M. Ismail, A. Sh. Ghazal, H. Abu Zahra, *J. Phys. G* **25**, 2137 (1999).

[18] C.Y. Wong, *Phys. Rev. Lett.* **31**, 766 (1973).

[19] S. Kailas, *Phys. Rep.* **284**, 381 (1997).